JOURNAL OF GEOPHYSICAL RESEARCH: ATMOSPHERES, VOL. 118, 11,419–11,428, doi:10.1002/jgrd.50845, 2013

Comparison of modeled and observed effects of radiation belt electron precipitation on mesospheric hydroxyl and ozone

Pekka T. Verronen,[1] Monika E. Andersson,[1] Craig J. Rodger,[2] Mark A. Clilverd,[3] Shuhui Wang,[4] and Esa Turunen[5]

Received 14 March 2013; revised 11 September 2013; accepted 16 September 2013; published 7 October 2013.

[1] Observations have shown that mesospheric hydroxyl (OH) is affected by energetic electron precipitation (EEP) at magnetic latitudes connected to the outer radiation belt. It is not clear, however, if the current satellite-based electron flux observations can be used to accurately describe EEP in atmospheric models. We use the Sodankylä Ion and Neutral Chemistry (SIC) model to reproduce the changes in OH and ozone observed by the Microwave Limb Sounder (MLS/Aura) during four strong EEP events. The daily mean electron energy-flux spectrum, needed for ionization rate calculations, is determined by combining the Medium Energy Proton and Electron Detector fluxes and spectral form from the instrument for the detection of particles high-energy electron detector on board the DEMETER satellite. We show that in general SIC is able to reproduce the observed day-to-day variability of OH and ozone. In the lower mesosphere, the model tends to underestimate the OH concentration, possibly because of uncertainties in the electron spectra for energies >300 keV. The model predicts OH increases at 60–80 km, reaching several hundred percent at 70–80 km during peak EEP forcing. Increases in OH are followed by ozone depletion, up to several tens of percent. The magnitude of modeled changes is similar to those observed by MLS and comparable to effects of individual solar proton events. Our results suggest that the combined satellite observations of electrons can be used to model the EEP effects above 70 km during geomagnetic storms, without a need for significant adjustments. However, for EEP energies >300 keV impacting altitudes <70 km, correction factors may be required.

Citation: Verronen, P. T., M. E. Andersson, C. J. Rodger, M. A. Clilverd, S. Wang, and E. Turunen (2013), Comparison of modeled and observed effects of radiation belt electron precipitation on mesospheric hydroxyl and ozone, *J. Geophys. Res. Atmos.*, *118*, 11,419–11,428, doi:10.1002/jgrd.50845.

1. Introduction

[2] The odd hydrogen family ($HO_x = H + OH + HO_2$) plays an important role in the mesospheric O_3 balance by participating in catalytic ozone-destroying reactions and in reactions between different forms of other ozone-depleting compounds. However, continuous satellite observations of OH and HO_2 became available less than 10 years ago, after the launch of the Microwave Limb Sounder (MLS/Aura) instrument in 2004 [*Pickett et al.*, 2008]. In the mesosphere, the primary HO_x production mechanism is photodissociation of water vapor by solar radiation ($\lambda < 200$ nm) and its loss is due to "cannibalistic" reactions such as $OH + HO_2 \rightarrow H_2O + O_2$. The OH concentration increases by roughly an order of magnitude during daytime, except in a narrow layer around 82 km where a reaction between ozone and atomic hydrogen creates a nighttime OH maximum [*Pickett et al.*, 2006]. In the polar regions, enhancements of HO_x occur during energetic particle precipitation events, when increases in ionization rates lead to odd hydrogen production through ionization and water cluster ion chemistry [*Heaps*, 1978; *Solomon et al.*, 1981; *Verronen and Lehmann*, 2013]. Large changes are caused by solar proton events (SPE), during which high fluxes of highly energetic protons, related to coronal mass ejections from Sun, can affect the mesosphere and upper stratosphere for several days. For example, in the case of the January 2005 SPE, order-of-magnitude OH increases have been observed at 60–80 km, with subsequent decreases in ozone by 50–90% [*Verronen et al.*, 2006; *Damiani et al.*, 2008]. Energetic particle precipitation can increase HO_x below about 80 km, where there is enough H_2O for water cluster ion formation. At these altitudes, the nighttime background concentration of HO_x is low and its chemical lifetime varies

[1] Earth Observation, Finnish Meteorological Institute, Helsinki, Finland.
[2] Department of Physics, University of Otago, Dunedin, New Zealand.
[3] British Antarctic Survey (NERC), Cambridge, UK.
[4] Jet Propulsion Laboratory, California Institute of Technology, Pasadena, California, USA.
[5] Sodankylä Geophysical Observatory, University of Oulu, Sodankylä, Finland.

Corresponding author: P. T. Verronen, Earth Observation, Finnish Meteorological Institute, P.O. Box 503, FI-00101 Helsinki, Finland. (pekka.verronen@fmi.fi)

2169-897X/13/10.1002/jgrd.50845

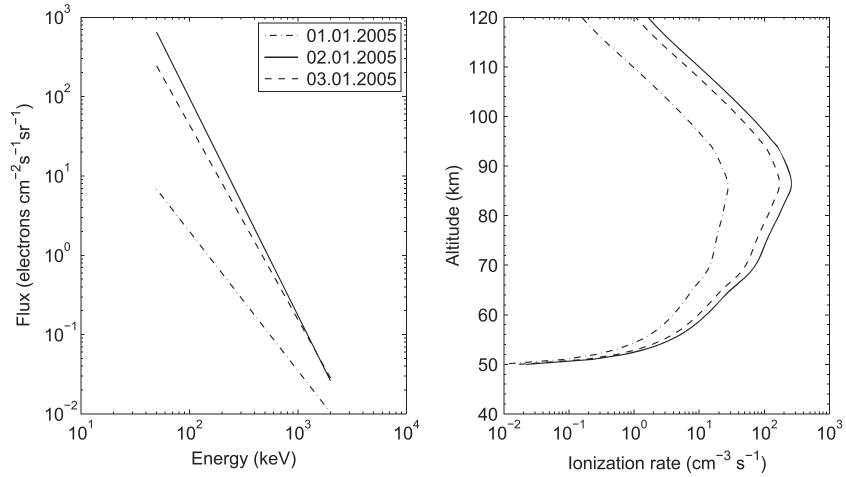

Figure 1. (left) EEP flux-energy spectra on selected days in January 2005. (right) Corresponding calculated atmospheric ionization rate profiles for the Northern Hemisphere modeling location.

between 0.1 and 1 day [e.g., *Pickett et al.*, 2006]. This means that HO_x is a useful monitor species for short-term precipitation variations, because its concentration responds rapidly to both increases and decreases in particle forcing [*Damiani et al.*, 2010; *Verronen et al.*, 2011].

[3] Recent observational studies using data from the Medium Energy Proton and Electron Detector (MEPED/POES) and Microwave Limb Sounder (MLS/Aura) have shown that radiation belt electrons, precipitating into the atmosphere during magnetic storms, have a significant effect on mesospheric nighttime hydroxyl concentrations at magnetic latitudes between 55° and 72°. *Verronen et al.* [2011] studied 2 months, March 2005 and April 2006, and found a significant correlation between electron count rates and hydroxyl in both hemispheres providing some of the first experimental evidence that electron precipitation could produce significant HO_x changes. Electron precipitation was shown to cause day-to-day OH changes up to 100% and explain 56–87% of the OH variability. *Andersson et al.* [2012] extended the correlation study and analyzed 65 months between 2004 and 2009. In about 34% of the time, they found a clear correlation between electron counts and hydroxyl concentrations. In both studies, the largest OH response was seen at 70–78 km altitude, while below 50 km and above 80 km no correlation was found.

[4] The relation between the electron counts measured in the radiation belts and the precipitating electron fluxes is in many cases not trivial, because satellite instruments, such as MEPED/POES, typically measure only a fraction of the precipitation and the electron measurements can be contaminated by protons [*Rodger et al.*, 2010a]. Recent studies using ground-based measurements have indicated that an adjustment of >30 keV electron fluxes, up to a factor of 10, may be needed in order to produce the observed ionospheric response in models [*Hendry et al.*, 2012; *Clilverd et al.*, 2012]. However, because the ground-based instruments used in these studies can monitor an altitude-integrated response only, it is not clear if the required adjustment depends on electron energy. On the other hand, it is increasingly likely that an adjustment is needed for electron energies >300 keV. According to radiation belt models (R.B. Horne, private communication, 2013), when electron energy increases toward MeV level, there is increasingly uneven effect of wave-particle scattering on the bounce loss cone (BLC). This means that the distribution of electrons with a given energy changes inside the BLC. As a result, a satellite instrument sampling only a fraction of the BLC, such as MEPED, is likely to miss a larger part of precipitating electrons at high energies.

[5] In this paper, we use the Sodankylä Ion and Neutral Chemistry (SIC) model to study the effect of precipitating radiation belt electrons on mesospheric OH and O_3. The electron spectra input to the model was calculated using flux observations of MEPED/POES and a power law form previously found to be appropriate using data from the IDP (instrument for the detection of particles) high-energy electron detector on board the DEMETER (Detection of Electromagnetic Emissions Transmitted from Earthquake Regions) microsatellite [*Clilverd et al.*, 2010]. A detailed comparison between the model results and OH observations from MLS/Aura allows us to test the quality of the electron spectra at different electron energies.

Table 1. Details of the Monthly Cases[a]

Month	Modeling Period (day)	Modeling Locations (geographic)	EEP Peak Day (day)	RD (day)	Number of MLS Profiles (NH/SH)
January 2005	01–10	60°N/0°E, 50°S/105°E	02	01	57–68/18–24
March 2005	05–10	60°N/0°E, 65°S/0°E	07	05	95–105/52–69
May 2005	25–31	55°N/75°W, 65°S/0°E	30	29	13–19/97–112
April 2006	13–17	60°N/0°E, 65°S/0°E	14	12	20–33/72–84

[a]RD is the reference day that was used when calculating observed and modeled changes. For all modeling locations, the geomagnetic latitude is about 60°.

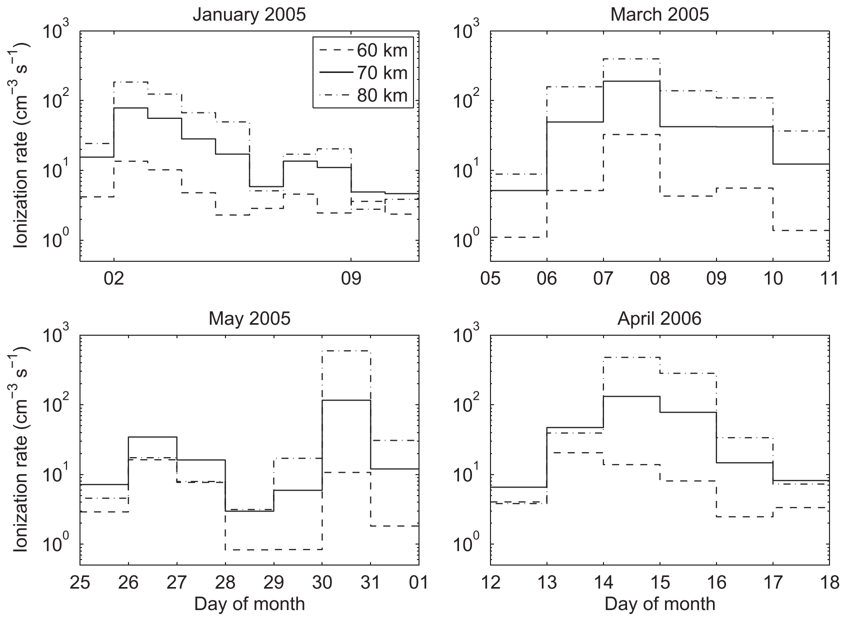

Figure 2. Calculated daily mean EEP ionization rates at selected altitudes for the NH modeling locations.

2. Modeling, Measurements, and Comparison

[6] Between 2004 and 2009, there were several energetic electron precipitation (EEP) events which had a clear effect on mesospheric hydroxyl [*Andersson et al.*, 2012]. In this work we consider four of the strongest events that occurred during this time period: January, March, May 2005, and April 2006. These events were selected to provide the most detectable electron forcing on the middle atmosphere and thus are best suited for our purpose of testing the quality of the satellite-based electron fluxes. Also, these time periods are not affected by SPEs, during which the electron flux measurements are corrupted by protons [*Rodger et al.*, 2010a].

2.1. Sodankylä Ion and Neutral Chemistry Model

[7] The Sodankylä Ion and Neutral Chemistry model is a one-dimensional tool designed for ionospheric and middle atmospheric studies. The latest version solves the concentrations of 65 ions, including 29 negative ions and 16 neutral species between 20 and 150 km altitude (1 km resolution). A chemical scheme of about 400 reactions is included (including standard O_x, HO_x, and NO_x neutral chemistry), as well as external forcing by solar radiation (ultraviolet, visible, and soft X-ray), electron and proton precipitation, and galactic cosmic rays. In this study, the temporal resolution was selected to be 15 min. A more detailed description of SIC is given elsewhere [*Verronen et al.*, 2005; *Verronen*, 2006; *Turunen et al.*, 2009].

[8] Considering the effects of electron precipitation, in the SIC model the calculation of ionization rates uses an experimental energy dissipation function and energy range relation for electrons (see *Rees* [1989, Chapter 3.3] for more details). The dissipation function assumes an isotropic angular distribution, and the range of electrons is calculated using the expression given by *Goldberg et al.* [1984]. The chemical production of HO_x species in the model, after ionization takes place, involves dissociation of H_2O, water cluster ion formation through positive ion chemistry, and recombination processes which lead to OH and H production [*Verronen and Lehmann*, 2013]. The produced HO_x then affects ozone in the mesosphere through the well-known catalytic reaction cycles of neutral chemistry [e.g., *Grenfell et al.*, 2006].

[9] The ionization rate calculation requires an energy-flux spectrum of electrons. In construction of the spectra, we combined observations from two satellite instruments: MEPED/POES and IDP/DEMETER [*Evans and Greer*, 2004; *Sauvaud et al.*, 2006]. MEPED observations are available for three energy threshold channels, >30 keV, >100 keV, and >300 keV, from three different POES satellites. We utilized data from magnetic latitudes 55 – 65° (McIlwain L shells 3.0–5.7) gathered by the 0° detector, which points radially outward along the Earth satellite direction and measures count rates of precipitating radiation belt electrons [*Rodger et al.*, 2010a, 2010b]. Following the previous work in this area [*Verronen et al.*, 2011; *Andersson et al.*, 2012; *Hendry et al.*, 2012], we exclude fluxes from the South Atlantic region, where the instrument is contaminated by high-energy protons. We then calculated daily zonal mean of the electron fluxes for the three MEPED energy channels and used them to fit an energy spectrum. The spectral form of the fit is based on the power law relationship previously found to be appropriate using observations of the IDP instrument [*Clilverd et al.*, 2010]. IDP has 128 energy channels and thus a vastly better energy resolution compared to the three integral channels from MEPED. However, IDP does not measure precipitating electrons but electrons in the drift loss cone, i.e., electrons that have a pitch angle close to the precipitation limit but which drift around the Earth to be lost where the magnetic field is weakest (in the South Atlantic). Therefore, our assumption is

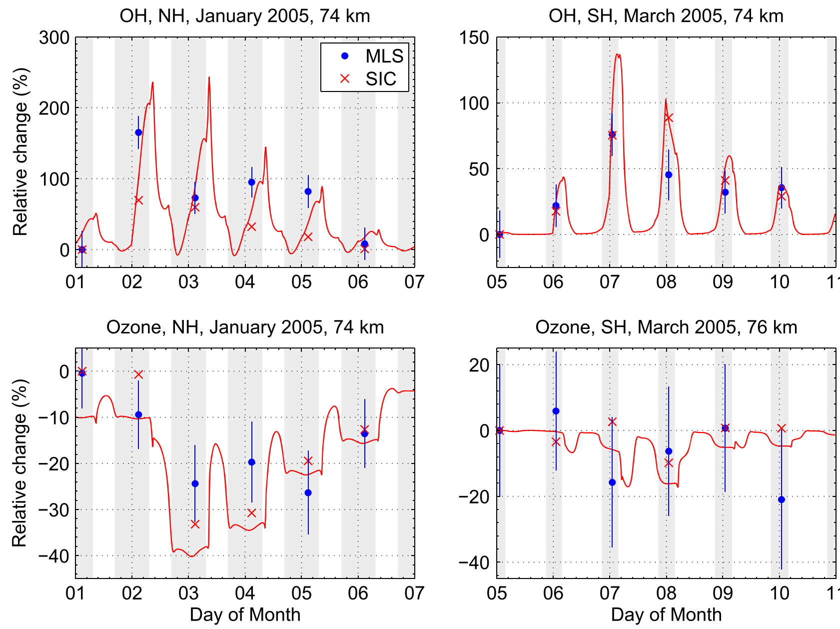

Figure 3. Comparison between modeled and observed EEP-caused relative change of OH and ozone at about 75 km for January NH (left) and March SH (right) 2005. Red lines denote the SIC data showing 100 × (EEP/CTR - 1), where EEP and CTR are gas concentrations from the electron and control runs, respectively. Red X marks are the same as the red lines, except that CTR is replaced by first day result from the EEP run and shown only at the LST of MLS observations. Blue circles denote MLS data showing the change with respect to the observations on the day before EEP peak (see Table 1). Gray shading marks are the local times with solar zenith angle larger than 100°, i.e., approximately nighttime.

that the precipitating electrons have same spectral form as those in the drift loss cone, as they are very close in pitch angle space.

[10] Figure 1 shows examples of electron energy spectra (left) and ionization rates (right) for three different days in January 2005: before (1 January), during (2 January), and after (3 January) an EEP event. The flux on 2 January exceeds the 1 January flux by almost two orders of magnitude at the lower energies, while at the highest energies there is an increase by a factor of three. When the electron flux peaks, ionization rates are about 10 times higher than the values before the peak EEP, with the maximum increase between 70–100 km. It is important to note that the atmospheric penetration depth of an electron depends on its energy [e.g., *Turunen et al.*, 2009, Figure 3]. As shown in Figure 1, the calculated ionization rate is always zero below 50 km because we do not consider electrons with energies larger than 2000 keV, which would penetrate to stratospheric altitudes. This upper energy limit is set by the MEPED and IDP measurements, because both instruments respond to electron energies less than about 2500 keV only [*Evans and Greer*, 2004]. The lower limit of electron energy is set at 50 keV in order to capture the EEP effect at altitudes below about 90 km.

[11] The times and locations of the model runs are given in Table 1. For each of the four cases, the SIC model was run for two geographic locations, one in the Northern Hemisphere (NH) and one in the Southern Hemisphere (SH). These locations are at about 60°N/S geomagnetic latitude, which connects to the center of the outer radiation belt via magnetic field lines. For each location/month, two model runs were made: (1) an EEP run with the observed, daily average EEP forcing and (2) a CTR (control) run with low and constant EEP forcing corresponding to quiet time conditions (defined as the average of 3–4 March 2005). MLS/Aura observations of water vapor (H_2O) and temperature (T), monthly averaged for each case separately, were used in the SIC modeling to provide more realistic atmospheric conditions. The rest of the background neutral atmosphere and daily solar flux spectrum were generated using the MSISE-90 and the SOLAR2000 models, respectively [*Hedin*, 1991; *Tobiska et al.*, 2000]. To make the model results and satellite measurements comparable, OH and O_3 altitude profiles from SIC were interpolated to the logarithmic pressure grid of MLS observations. Then, the MLS averaging kernel was applied to O_3 profiles from SIC to compensate for the coarser vertical resolution of the MLS observations [see *Livesey et al.*, 2011, for more details]. The vertical resolution of MLS OH observations is closer to the 1 km model resolution, i.e., 2.5 km at all altitudes below 80 km, and thus, the OH averaging kernel was not applied to model results because its effect would be small. Note that the results are presented on a vertical grid of approximate altitudes, which correspond to the pressure levels of the MLS observations.

2.2. Observations of Hydroxyl and Ozone

[12] The MLS instrument on board the Aura satellite was launched in July 2004 [*Waters et al.*, 2006]. The Aura satellite is in a high-inclination orbit, and the MLS observations cover the polar regions (geographic latitudes less than 82°). Detailed information on the MLS OH and O_3 products can be found elsewhere [*Pickett et al.*, 2008; *Jiang et al.*, 2007; *Livesey et al.*, 2011]. We use Version 3.3 Level 2 nighttime

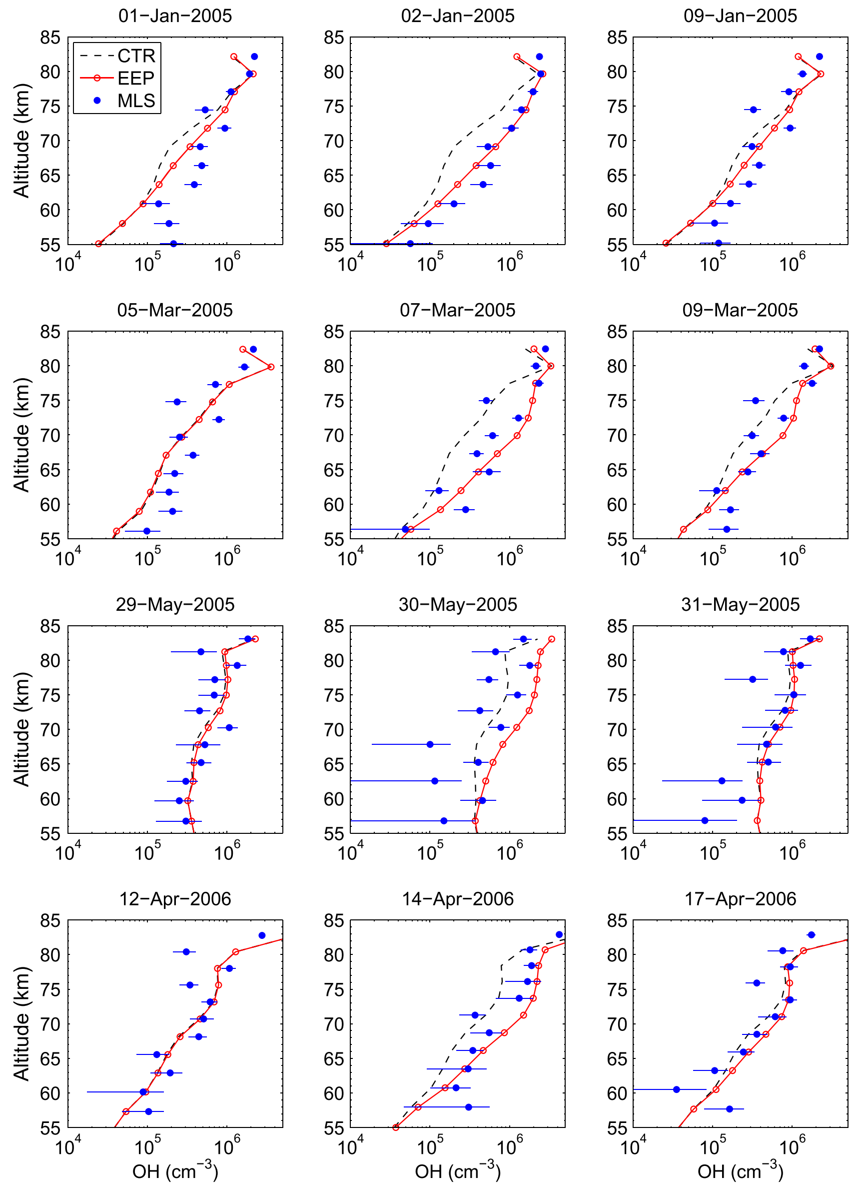

Figure 4. Comparison of NH modeled and observed nighttime OH concentrations (left) before, (middle) during, and (right) after the peak EEP day. (top to bottom) January 2005, March 2005, May 2005, and April 2006. Black, red, and blue colors mark the data from SIC CTR run, SIC EEP run, and MLS observations, respectively.

(solar zenith angle $\geq$ 100°) data from geomagnetic latitudes 59–65° from both hemispheres. At these latitudes, MLS nighttime observations correspond to local times of 22:00–02:00 and 02:00–03:30 in the SH and NH, respectively. Before the analysis, the data were screened according to the MLS data description and quality document [*Livesey et al.*, 2011]. We then calculated nightly zonal averages and corresponding SEMs (standard error of the mean) at each pressure level of MLS observations. The number of individual profiles used in calculating the means varied between 100 (NH) in January to 15 (NH) in May (see Table 1). Due to the incomplete nighttime zonal coverage in January SH and May NH, the longitudinal range was limited to 0–180° E and 0–180° W, respectively. For these two cases, the model runs were made at 50°S/105°E (January) and at 55°N/75°W (May), according to the radiation belt position at these longitudes.

[13] We have chosen to work with daily zonal averages instead of a finer temporal and spatial resolution. This approach reduces uncertainties of the observational data to an acceptable level but, on the other hand, it restricts us from fine detail comparisons between the SIC model and MLS observations. However, since the aim is to understands if large corrections (e.g., scaling factors of 10) are needed for the electron flux data, the current approach is appropriate for this study. For a given geographic latitude, the MLS observations have the same local solar time (LST) at all longitudes. So daily zonal averages only include observations of about the same LST (the LST range depending on the latitude range selection). Because we force the model

Table 2. Observed (MLS) and Modeled (SIC) OH Changes Caused by the Peak EEP Day Forcing in the Northern Hemisphere[a]

Alt (km)	MLS 60–70	MLS 71–81	SIC 60–70	SIC 71–81
02 Jan 2005	0.8 (24%)	6.0 (70%)	1.5 (67%)	6.1 (65%)
07 Mar 2005	1.6 (67%)	7.2 (108%)	4.7 (240%)	8.5 (200%)
30 May 2005	–2.1 (–30%)	2.6 (34%)	5.5 (94%)	12.7 (140%)
14 Apr 2006	0.7 (55%)	10.9 (266%)	5.1 (179%)	14.4 (240%)

[a]Both absolute (in units 10^5 cm^{-3}) and relative changes (in brackets) are shown. Columns from left to right denote (1) EEP peak day, (2) observed mean change at 60–70 km, (3) observed mean change at 71–81 km, (4) modeled mean change at 60–70 km, and (5) modeled mean change at 71–81 km. The SIC changes (columns 4 and 5) are calculated from the EEP run results. Both SIC and MLS changes are relative to the day before, as indicated in Table 1 (reference day). The SEM of the MLS numbers varies between 15 and 45%.

with daily zonal mean electron fluxes, the model results at different longitudes (but sampled at the same LST) would not be significantly different. Thus, the model results from one longitude are comparable to the daily zonal mean of MLS observations. Note that HO_x production is nearly linear with respect to particle ionization rate (although the HO_x production efficiency does decrease slowly with increasing ionization [see, e.g., *Verronen and Lehmann*, 2013]), which means that the daily average ionization rates produce a modeled OH result that should be very similar to daily average OH results produced using a finer temporal resolution for the ionization rates.

3. Results

[14] Figure 2 shows the temporal variation of the calculated NH daily EEP ionization rates at 60, 70, and 80 km. In all four cases there are substantial day-to-day variations in ionization, which should lead to observable changes in mesospheric OH concentrations. On quiet days the ionization rates are between 1 and 10 cm^{-3}s^{-1} at all altitudes shown, while the peak ionization during EEP events can exceed 10^2 cm^{-3}s^{-1}. For comparison, the ionization by solar Lyman-α radiation and galactic cosmic rays typically varies between 0.1 and 10 cm^{-3}s^{-1} at these altitudes, and during very large SPEs the daily average ionization rate can be higher than 10^3 cm^{-3}s^{-1}. Therefore, the peak EEP ionization rates are clearly higher than the normal background but are still about an order of magnitude lower than for the largest SPEs.

[15] Figure 3 presents a comparison between the modeled and observed EEP-related relative changes of OH and O_3 at about 75 km altitude for two of the cases: January 2005/NH and March 2005/SH, which represent the magnitude range of the EEP effects. For the model results, the change is shown (1) between the EEP and CTR runs (red line) and (2) between the EEP run and the first day value of the EEP run (red X marks, only for the LST of MLS observations).

[16] First looking at the modeled change with CTR run as a reference, the model results clearly show how the relative change is dependent on local time. For example, the largest OH increases are seen in the early morning hours, around sunrise, when the background OH concentration is lowest. In March 2005/SH, when the noon solar zenith angle is much lower than in January, the noontime OH increase is negligible, i.e., of the order of 1%. Also, the ozone change is dependent on the local time; its depletion taking place at sunrise and sunset when (1) HO_x concentration is elevated by EEP and (2) enough atomic oxygen is available for the ozone-destroying catalytic HO_x reaction cycles (note that the sunrise decrease of ozone is not always seen in Figure 3 because a decrease in daily EEP forcing from the previous day can lead to ozone recovery at sunrise). Thus, the largest ozone changes do not necessarily coincide with the largest OH changes. At night, no significant production or loss of O_3 takes place because of the absence of solar radiation and atomic oxygen. Contrary to the model results, the observations are only available at certain local times, as shown in Figure 3. In the case of OH, the model results are in general agreement with the observations, predicting maximum increases that reach 80–100% at the local time of the observations. However, in January/NH SIC tends to underestimate the EEP impact (MLS shows increase by 165% on 2 January), and in March/SH the model is overestimating the change on 8 March. However, on many days the data points agree or nearly agree within the SEM of the observations (shown by the error bar in Figure 3). For ozone, the modeled depletion is up to 40% and 16% in January/NH and March/SH, respectively, varying from day to day with the level of EEP forcing and the related OH change. The observations do show a smaller decrease in January/NH, up to 25–30% only, but qualitatively, the day-to-day behavior (depletion and recovery) is similar to the model in both cases. Note that the SEM of the ozone observations in March/SH is larger than the predicted changes.

Table 3. Differences Between Modeled (CTR and EEP Runs) and Observed (MLS) OH Concentrations, Averaged Between 60 and 78 km[a]

		CTR versus MLS 10^5 cm^{-3} (%)	EEP versus MLS 10^5 cm^{-3} (%)
02 Jan 2005	NH	4.7 (–59)	1.2 (–11)
	SH	8.1 (–23)	6.3 (+8)
07 Mar 2005	NH	5.3 (–54)	3.1 (+44)
	SH	6.6 (–52)	3.7 (–17)
30 May 2005	NH	3.7 (+46)	8.0 (+219)
	SH	3.8 (–47)	2.5 (–10)
14 Apr 2006	NH	4.8 (–40)	4.5 (+70)
	SH	4.5 (–45)	2.4 (–12)

[a]Absolute differences are calculated as abs(SIC – MLS) and relative differences as 100 × (SIC/MLS – 1). For each month, the upper line is for NH and the lower line for SH.

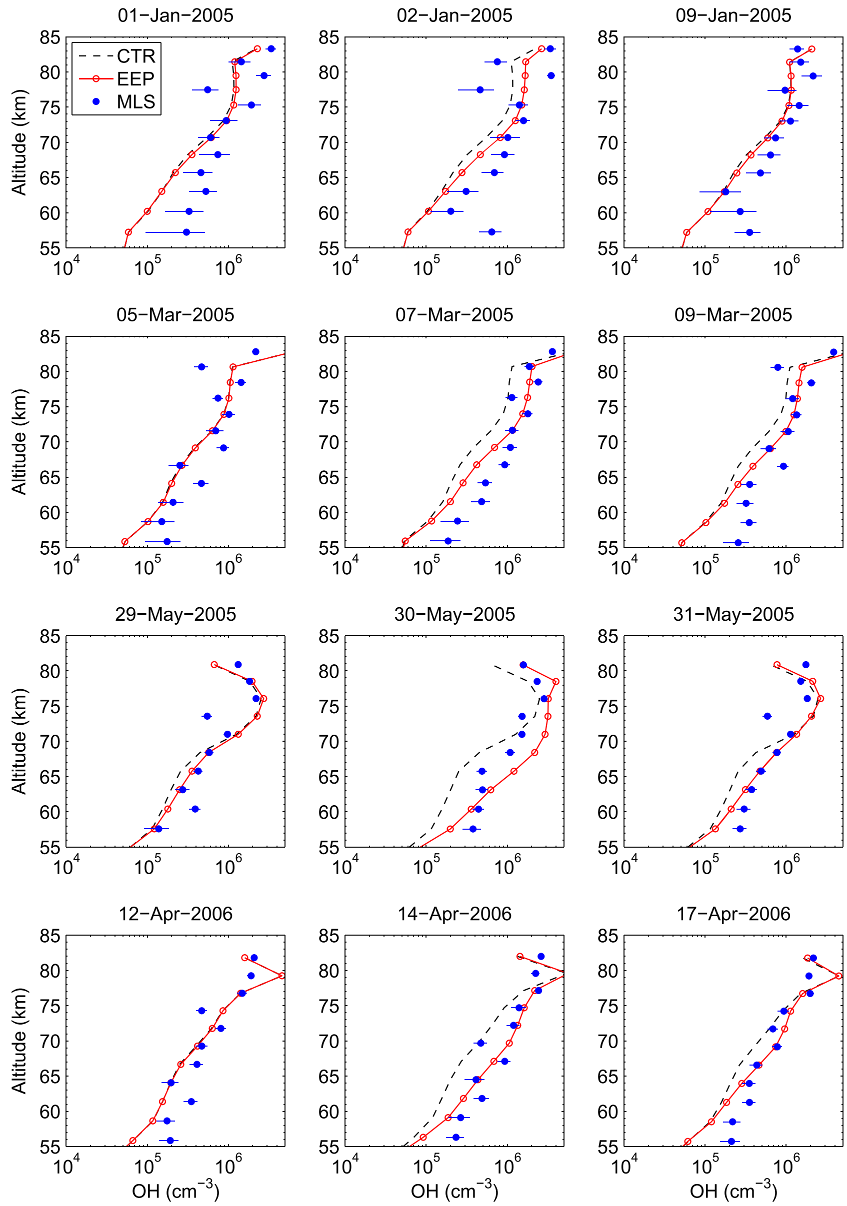

Figure 5. Similar to Figure 4 but for SH.

[17] When the modeled changes are shown relative to the first day value (1 January and 5 March), in January/NH both the OH increase and ozone depletion are smaller than when using CTR run as a reference. This is because the EEP ionization rates are already elevated on 1 January (Figure 2). The maximum OH increase on 2 January is 70%, which is again smaller than that observed. On the other hand, the ozone change is in a better agreement with MLS although still overestimated on 3 and 4 January. In March/SH, the modeled OH change is not much different compared to that relative to the CTR run. The ozone change is different because the day-to-day background variability is comparable to that driven by EEP. In this case, the CTR run reference gives a better estimate of ozone changes, because it removes the underlying day-to-day variability.

[18] Figure 4 shows the NH comparisons between SIC and MLS daily concentration profiles (1) before, (2) during, and (3) after the peak EEP day. In all cases, the modeled OH concentrations are elevated on the peak EEP day compared to the day before and then at least partly recover on the following day. Largest effects are seen at altitudes between 60 and 80 km. Although there are clear differences in absolute numbers between MLS and SIC at a number of altitudes, the model seems to be able to qualitatively represent most of the observed day-to-day changes in OH. Table 2 presents the observed and modeled NH mean OH increase from the

Table 4. Similar to Table 2 but for Southern Hemisphere

Alt (km)	MLS 60–70	MLS 71–81	SIC 60–70	SIC 71–81
02 Jan 2005	3.7 (53%)	-1.5 (-17%)	1.7 (30%)	4.1 (33%)
07 Mar 2005	3.6 (94%)	8.9 (124%)	2.7 (65%)	7.8 (77%)
30 May 2005	2.1 (50%)	6.7 (73%)	7.5 (190%)	12.4 (70%)
14 Apr 2006	2.2 (69%)	6.4 (81%)	3.5 (130%)	8.1 (69%)

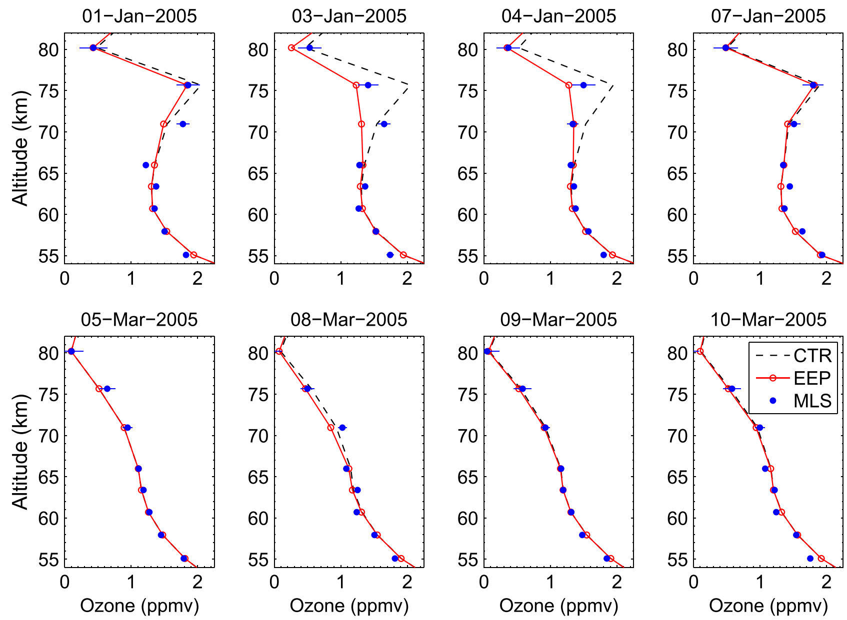

Figure 6. Comparison of modeled and observed nighttime ozone mixing ratios. (top row) January 2005, NH. (bottom row) March 2005, SH. Black, red, and blue colors mark the data from SIC CTR run, SIC EEP run, and MLS observations, respectively.

day before to peak EEP concentrations at 60–70 km and 71–81 km. In general, SIC tends to overestimate rather than underestimate the increase compared to MLS although the difference is only in tens of percent in most cases. At higher altitudes, this is caused in few cases by an overestimation of the EEP effect in the model (e.g., 14 April 2006 in Figure 4), while at lower altitudes the difference in relative change is at least partly due to lower reference concentrations (CTR) in SIC (e.g., 05 March 2005 in Figure 4). On 30 May 2005 the difference between SIC and MLS is especially large, the EEP model run predicting clearly larger amounts of OH than those observed. The larger differences could be related to the smaller amount of MLS measurements available for this month, because a nightly zonal mean calculated with limited number of available data points is less representative of the rapidly changing EEP effect. As shown in Table 3, on the EEP peak days the OH profiles from the EEP run agree with MLS observations better than those from the CTR run, except in May 2005.

[19] Figure 5 and Table 4 present the same comparison for the SH. In general, the absolute increase in OH is similar to that in the NH, both in observations and modeling, except that at 60–70 km MLS observes in all cases larger absolute OH increase than in the NH. The general agreement in OH change between the SIC EEP run and observations is better in the SH. However, again on 30-May-2005 the model clearly overestimates the OH concentration at all altitude between 65 and 75 km. Note that below 70 km, MLS OH concentrations are generally higher than values predicted by the model, this was also seen in some cases in the NH (Figure 4). In all cases, the MLS EEP peak day OH profiles agree better with the EEP run than with the CTR run (Table 3).

[20] The increase in HO_x leads to significant depletion of mesospheric ozone, as already shown in Figure 3. The observed and modeled O_3 mixing ratios are shown in Figure 6 for two cases: January 2005, NH, and March 2005, SH. The notable difference between the ozone altitude profiles is the tertiary ozone maximum around 75 km [e.g., *Sofieva et al.*, 2009, and references therein], which in our study is observed in January/NH but not in March/SH. In both cases, modeled ozone depletion is seen at altitudes above 65 km after the peak EEP days, but the March/SH changes are much smaller, because sunrise/sunset OH increases are modest compared to January/NH (Figure 3). The ozone results from the EEP model run are in agreement with observations at most altitudes, indicating a similar day-to-day variability with respect to EEP forcing. In January/NH, the maximum depletion is observed at 75 km, where a decrease of about 0.4 ppmv is seen on 3 and 4 January compared to 1 January, while there is a decrease of 0.5–0.6 ppmv in the EEP run results with respect to 1 January. By 7 January, the EEP forcing has declined from the peak values, and the ozone mixing ratios have returned close to the pre-EEP peak level. Compared to the CTR run results, those from the EEP run are clearly in better agreement with the MLS observations. In March/SH at 75 km, ozone depletion of up to 0.1 ppmv is observed on 8 and 9 March, compared to 5 March. However, although the EEP run results indicate a similar behavior, this change is smaller than the SEM of the observations. Observing effects of this magnitude is obviously challenging.

4. Discussion

[21] The SIC model is producing EEP-related OH changes that are comparable to those observed by MLS, and the effects are seen at altitudes between 60 and 80 km, which is in agreement with previous studies using only observations [*Verronen et al.*, 2011; *Andersson et al.*, 2012]. However, as shown in Figure 1, the calculated ionization rates fall off rapidly below 60 km, because of the applied

2 MeV upper limit for electron energies. As a result, the calculated EEP impact might be somewhat underestimated in the lower mesosphere, which could explain some of the OH underestimation in the model below 60 km. Although it is possible that the same spectral form is applicable for energies higher than 2 MeV too, the satellite-based electron data cannot be used to support or falsify this assumption.

[22] The agreement between the modeled and observed OH response indicates that by introducing the daily average electron flux-energy spectra, based on MEPED and IDP electron data, the EEP effect on the mesosphere can be modeled reasonably well. Note especially that, in general, the EEP-related change on the peak EEP day (relative to the day before) is overestimated also at lower altitudes (Tables 2 and 4), not underestimated. However, in 60–70% of the days shown in Figures 4 and 5 the model tends to underestimate the observed OH concentration (in absolute numbers) below 70 km, except in some cases where the EEP ionization is very low (e.g., 12 April 2006, NH, Figure 4). This could perhaps mean that the assumed spectral form leads to too low electron fluxes at higher energies and is consistent with the idea that an adjusting factor is required for higher energy electron precipitation (>300 keV electrons penetrate to altitudes below 70 km). Also, the fact that model-observation differences at <70 km altitudes occur also during moderate electron forcing is consistent with weak diffusion processes taking place in the radiation belts which will increase the satellite flux adjustment factor for >300 keV electrons during moderate forcing events [e.g., *Clilverd et al.*, 2012].

[23] On the other hand, the fact that in Figures 4 and 5 the model underestimation is sometimes seen with low electron forcing (e.g., 5 March 2005 NH and 12 April 2006 SH) might also suggest a reason other than incorrect EEP fluxes. For example, there are also uncertainties related to, e.g., the assumption of angular distribution of electrons, and the additional ionization by Bremsstrahlung X-ray radiation produced by precipitating electrons is not considered (which would add to the ionization at the lower altitudes, below the main ionization peak [see, e.g., *Schröter et al.*, 2006]). Considering also that at lower altitudes the EEP effect is expected to be relatively small and that there is generally less OH (which makes the observation noisier), the overall agreement in OH is quite reasonable. Therefore, there seems to be no need for substantial (e.g., factor of 10) corrections to the electron flux observations, as suggested before [*Hendry et al.*, 2012; *Clilverd et al.*, 2012], at least not in the energy range corresponding to the OH changes at 70–80 km. As a test, we multiplied the calculated electron flux values at all energies by a factor of 10 and repeated the modeling for the case of March 2005. The elevated fluxes resulted in significantly higher OH values from the model (not shown), with average difference between model and the observations at 60–78 km reaching 500%. This is obviously a poor agreement compared to that between the observations and the original EEP model results (Table 3).

[24] As shown in Figures 3 and 6, EEP events can cause short-term depletion of tens of percent in mesospheric ozone. These changes are similar to those caused by large SPEs, although having a somewhat smaller magnitude. For example, during the SPE of 18 January 2005, ozone was depleted by up to 90% at 70–80 km [e.g., *Verronen et al.*, 2006]. In our study, the largest ozone effect was seen in the NH for the January 2005 case. This is in agreement with previous studies of SPEs that have reported relatively larger ozone response in the winter pole, related to the hemispheric differences in background HO_x concentration [*Rohen et al.*, 2005; *Jackman et al.*, 2008; *Damiani et al.*, 2010].

[25] In a recent study, mesospheric hydroxyl observations from August 2004 to December 2009 indicated an observable response to EEP in 22 (34%) of the 65 months analyzed [*Andersson et al.*, 2012]. During the same time period, 13 SPEs of various magnitudes took place according to the NOAA Space Weather Prediction Center (http://www.swpc.noaa.gov/ftpdir/indices/SPE.txt, accessed in January 2013). Assuming that all 13 SPEs had an impact on the mesospheric OH concentrations, the rate of large enough EEP events exceeds the rate of hydroxyl-affecting SPEs by 70% during this time period. Therefore, it is reasonable to argue that on time scales of a solar cycle, the EEP forcing could be more important to mesospheric OH and ozone than SPEs. Obviously, longer time series of data, preferably covering several solar cycles, would be needed for more quantitative conclusions.

5. Summary

[26] We have used a 1-D ion and neutral chemistry model to study the effects of radiation belt electron precipitation in the middle atmosphere. We considered four events, each with high daily fluxes of precipitating electrons observed in the outer radiation belt. For the modeling, the energy-flux spectra of electrons, and subsequently, the atmospheric ionization rates, were calculated based on electron observations of the MEPED and IDP satellite instruments.

[27] The model results show that the energetic electron precipitation can have a significant effect on mesospheric OH and ozone. The maximum OH increase can reach several hundred percent, but the magnitude of the relative effect depends strongly on the solar zenith angle and the level of background OH production. Largest relative OH increases are seen in the winter pole and around sunrise. The OH enhancements lead to ozone depletion by up to several tens of percent, which is comparable to the effects previously reported in cases of large SPEs. In general, the model is able to reproduce the observed daily variability of OH and ozone, particularly at 70–80 km altitudes, although there are significant differences in absolute OH concentrations in the lower mesosphere. Some of the differences can be related to the assumptions made in the calculation of the electron spectra and atmospheric ionization rates. Nevertheless, the general agreement between the model and the observations indicate that the electron flux observations from satellites for energies < 300 keV can be used to model the atmospheric effects of EEP at 70–80 km, without a need for significant geometrical corrections. Some correction may be needed for energies > 300 keV, although at lower altitudes we cannot make any strong conclusion based on the current results.

[28] **Acknowledgments.** The work of P.T.V. and M.E.A was supported by the Academy of Finland through projects 136225 and 140888 (SPOC: Significance of Energetic Electron Precipitation to Odd Hydrogen, Ozone, and Climate). C.J.R. was supported by the New Zealand Marsden fund. Research at the Jet Propulsion Laboratory, California Institute of Technology is performed under contract with the National Aeronautics and Space Administration.

References

Andersson, M. E., P. T. Verronen, S. Wang, C. J. Rodger, M. A. Clilverd, and B. Carson (2012), Precipitating radiation belt electrons and enhancements of mesospheric hydroxyl during 2004–2009, *J. Geophys. Res.*, *117*, D09304, doi:10.1029/2011JD017246.

Clilverd, M. A., et al. (2010), Ground-based estimates of outer radiation belt energetic electron precipitation fluxes into the atmosphere, *J. Geophys. Res.*, *115*, A12304, doi:10.1029/2010JA015638.

Clilverd, M. A., C. J. Rodger, D. Danskin, M. E. Usanova, T. Raita, T. Ulich, and E. L. Spanswick (2012), Energetic particle injection, acceleration, and loss during the geomagnetic disturbances which upset Galaxy 15, *J. Geophys. Res.*, *117*, A12213, doi:10.1029/2012JA018175.

Damiani, A., M. Storini, M. Laurenza, and C. Rafanelli (2008), Solar particle effects on minor components of the Polar atmosphere, *Ann. Geophys.*, *26*, 361–370.

Damiani, A., M. Storini, C. Rafanelli, and P. Diego (2010), The hydroxyl radical as an indicator of SEP fluxes in the high-latitude terrestrial atmosphere, *Adv. Space Res.*, *46*, 1225–1235, doi:10.1016/j.asr.2010.06.022.

Evans, D. S., and M. S. Greer (2004), *Polar Orbiting Environmental Satellite Space Environment Monitor – 2 Instrument Descriptions and Archive Data Documentation*, NOAA Technical Memorandum version 1.4, Space Environment Laboratory, Colorado.

Goldberg, R. A., C. H. Jackman, J. R. Barcus, and F. Soraas (1984), Nighttime auroral energy deposition in the middle atmosphere, *J. Geophys. Res.*, *89*, 5581–5596.

Grenfell, J. L., R. Lehmann, P. Mieth, U. Langematz, and B. Steil (2006), Chemical reaction pathways affecting stratospheric and mesospheric ozone, *J. Geophys. Res.*, *111*, D17311, doi:10.1029/2004JD005713.

Heaps, M. G. (1978), The effect of a solar proton event on the minor neutral constituents of the summer polar mesosphere, *Tech. Rep. ASL-TR0012*, U.S. Army Atmos. Sci. Lab., White Sands Missile Range, N. M.

Hedin, A. E. (1991), Extension of the MSIS thermospheric model into the middle and lower atmosphere, *J. Geophys. Res.*, *96*, 1159–1172.

Hendry, A. T., C. J. Rodger, M. A. Clilverd, N. R. Thomson, S. K. Morley, and T. Raita (2012), Rapid radiation belt losses occurring during high speed solar wind stream driven storms: Importance of energetic electron precipitation, in *Dynamics of the Earth's Radiation Belts and Inner Magnetosphere, American Geophysical Union Monograph,* vol. 199, edited by D. Summers et al., pp. 213–223, AGU, Washington, D.C. doi:10.1029/2012GM001299.

Jackman, C. H., et al. (2008), Short- and medium-term atmospheric constituent effects of very large solar proton events, *Atmos. Chem. Phys.*, *8*, 765–785, doi:10.5194/acp-8-765-2008.

Jiang, Y. B., et al. (2007), Validation of Aura Microwave Limb Sounder ozone by ozonesonde and lidar measurements, *J. Geophys. Res.*, *112*, D24S34, doi:10.1029/2007JD008776.

Livesey, N. J., et al. (2011), *EOS MLS Version 3.3 Level 2 data quality and description document,* JPL D-33509, Jet Propulsion Laboratory, Version 3.3x-1.0, January, 18.

Pickett, H. M., W. G. Read, K. K. Lee, and Y. L. Yung (2006), Observation of night OH in the mesosphere, *Geophys. Res. Lett.*, *33*, L19808, doi:10.1029/2006GL026910.

Pickett, H. M., et al. (2008), Validation of Aura Microwave Limb Sounder OH and HO_2 measurements, *J. Geophys. Res.*, *113*, D16S30, doi:10.1029/2007JD008775.

Rees, M. H. (1989), *Physics and Chemistry of the Upper Atmosphere, Cambridge Atmospheric and Space Science Series*, Cambridge Univ. Press, Cambridge, UK.

Rodger, C. J., M. A. Clilverd, J. C. Green, and M. M. Lam (2010a), Use of POES SEM-2 observations to examine radiation belt dynamics and energetic electron precipitation into the atmosphere, *J. Geophys. Res.*, *115*, A04202, doi:10.1029/2008JA014023.

Rodger, C. J., B. R. Carson, S. A. Cummer, R. J. Gamble, M. A. Clilverd, J.-A. Sauvaud, M. Parrot, J. C. Green, and J.-J. Berthelier (2010b), Contrasting the efficiency of radiation belt losses caused by ducted and non-ducted whistler mode waves from ground-based transmitters, *J. Geophys. Res.*, *115*, A12208, doi:10.1029/2010JA015880.

Rohen, G., et al. (2005), Ozone depletion during the solar proton events of October/November 2003 as seen by SCIAMACHY, *J. Geophys. Res.*, *110*, A09S39, doi:10.1029/2004JA010984.

Sauvaud, J. A., et al. (2006), High-energy electron detection onboard DEMETER: The IDP spectrometer, description and first results on the inner belt, *Planet. Space Sci.*, *54*, 502–511.

Schröter, J., B. Heber, F. Steinhilber, and M. Kallenrode (2006), Energetic particles in the atmosphere: A Monte Carlo simulation, *Adv. Space Res.*, *37*, 1597–1601, doi:10.1016/j.asr.2005.05.085.

Sofieva, V. F., et al. (2009), Spatio-temporal observations of the tertiary ozone maximum, *Atmos. Chem. Phys.*, *9*, 4439–4445, doi:10.5194/acp-9-4439-2009.

Solomon, S., D. W. Rusch, J.-C. Gérard, G. C. Reid, and P. J. Crutzen (1981), The effect of particle precipitation events on the neutral and ion chemistry of the middle atmosphere: II. Odd hydrogen, *Planet. Space Sci.*, *8*, 885–893.

Tobiska, W. K., T. Woods, F. Eparvier, R. Viereck, L. D. B. Floyd, G. Rottman, and O. R. White (2000), The SOLAR2000 empirical solar irradiance model and forecast tool, *J. Atmos. Sol.-Terr. Phys.*, *62*, 1233–1250.

Turunen, E., P. T. Verronen, A. Seppälä, C. J. Rodger, M. A. Clilverd, J. Tamminen, C.-F. Enell, and T. Ulich (2009), Impact of different precipitation energies on NO_x generation during geomagnetic storms, *J. Atmos. Sol. Terr. Phys.*, *71*, 1176–1189, doi:10.1016/j.jastp.2008.07.005.

Verronen, P. T. (2006), *Ionosphere-Atmosphere Interaction During Solar Proton Events*, no. 55 in Finnish Meteorological Institute Contributions, Finnish Meteorological Institute, Helsinki, Finland. URL: http://urn.fi/URN:ISBN:952-10-3111-5.

Verronen, P. T., and R. Lehmann (2013), Analysis and parameterisation of ionic reactions affecting middle atmospheric HO_x and NO_y during solar proton events, *Ann. Geophys.*, *31*, 909–956, doi:10.5194/angeo-31-909-2013.

Verronen, P. T., A. Seppälä, M. A. Clilverd, C. J. Rodger, E. Kyrölä, C.-F. Enell, T. Ulich, and E. Turunen (2005), Diurnal variation of ozone depletion during the October–November 2003 solar proton events, *J. Geophys. Res.*, *110*, A09S32, doi:10.1029/2004JA010932.

Verronen, P. T., A. Seppälä, E. Kyrölä, J. Tamminen, H. M. Pickett, and E. Turunen (2006), Production of odd hydrogen in the mesosphere during the January 2005 solar proton event, *Geophys. Res. Lett.*, *33*, L24811, doi:10.1029/2006GL028115.

Verronen, P. T., C. J. Rodger, M. A. Clilverd, and S. Wang (2011), First evidence of mesospheric hydroxyl response to electron precipitation from the radiation belts, *J. Geophys. Res.*, *116*, D07307, doi:10.1029/2010JD014965.

Waters, J. W., et al. (2006), The Earth Observing System Microwave Limb Sounder (EOS MLS) on the Aura satellite, *IEEE Trans. Geosci. Remote Sens.*, *44*, 1075–1092, doi:10.1109/TGRS.2006.873771.